

NUMERICAL MODELS FOR THE HYDROTHERMAL FIELD
AT THE GALAPAGOS SPREADING CENTER

Udo Fehn,¹ K. E. Green,² R. P. Von Herzen,³
and L. M. Cathles⁴

Abstract. The heat flow distribution at the Galapagos Spreading Center is compared to results of two-dimensional numerical models for the hydrothermal convection through oceanic crust. The model calculations are based on the equations for fluid flow through porous media adapted for the situation at spreading oceanic ridges. The temperature- and pressure-dependent thermodynamic characteristics of water were used in the fluid flow equations. Models with average permeabilities of approximately $5 \times 10^{-15} \text{ m}^2$ and penetration depths between 2 and 5 km produce heat flow distributions compatible with the observations at the Galapagos Spreading Center. Because of the convective heat loss, temperatures within the hydrothermal layer are significantly lower than for conductively cooling crust. Two different types of convection cells develop. The one or two cells closest to the ridge axis are fixed in location with respect to the ridge axis. Convection there is characterized by high temperatures ($>300^\circ\text{C}$), rapid flow rates, and low water to rock ratios (~ 1). These cells remove most of the heat associated with the intrusion process at the ridge axis. Cells farther away from the ridge axis move with the moving plate and serve to prevent the oceanic crust from reheating. Temperatures there typically are moderate to low ($<200^\circ\text{C}$), and flow velocities are lower than those in the axial cell, but water to rock ratios can be very high in these cells.

Introduction

In recent years the heat flow distribution at the Galapagos Spreading Center has been studied extensively [e.g., Williams et al., 1974; Green et al., 1981]. The distinct alternation found there between zones of high and low heat flow and, in addition, the difference between observed heat flow and that predicted by cooling plate models indicate that the heat flow distribution strongly reflects the influence of seawater circulation on the cooling process of the newly formed oceanic crust. Spectacular evidence for the presence of this hydrothermal convection came when hot springs at the ridge axis were discovered and investigated by using the sub-

mersible Alvin [e.g., Corliss et al., 1979].

Despite general acknowledgment of the role of hydrothermal convection in the formation of oceanic crust at the Galapagos Spreading Center and other active mid-ocean ridges, the mode and extent of this seawater penetration are not well understood. In this paper, we present the results of model calculations of fluid flow in the ocean crust and its effects on the surface heat flow and the cooling of young oceanic crust. The model is based on equations of flow through porous media, adapted to the situation at an active spreading center. The purposes of the calculation were (1) to test whether a model of this kind can simulate the observed heat flow distribution at the Galapagos Spreading Center, (2) to estimate the extent of the circulation, the depth of penetration, and the permeability distribution in the oceanic crust, (3) to investigate the stability of the circulation cells, and (4) to study the effect of convective heat transfer on the cooling history of the oceanic crust.

Geologic Setting

The area of investigation is located just south of the axis of the Galapagos Spreading Center. The geological and geophysical setting has been described in detail in several papers [e.g., Green et al., 1981; Crane and Ballard, 1980; Lonsdale and Klitgord, 1978; Hey, 1977], so that only the points relevant to our study will be mentioned here. The Galapagos Spreading Center has been spreading at a nearly constant rate of 3.5 cm/yr over at least the last 2 m.y. [Klitgord and Mudie, 1974]. It is characterized by a relatively smooth topography. Escarpments are, in general, parallel to the ridge axis and have offsets of usually less than 100 m [Allmendinger and Riis, 1979]. The water depth at the ridge crest is about 2500 m and increases over the survey area to nearly 3000 m, consistent with current plate tectonic models [Parsons and Sclater, 1977]. The sedimentation rate in the area is quite rapid, of the order of 50 m/m.y. so that a thin but relatively uniform sediment cover exists in the region. In the survey, which covers approximately 25 km x 30 km, more than 400 heat flow measurements were taken during several cruises. The heat flow distribution in the survey area is summarized in Figure 1, taken from Green et al [1981]. Heat flow measurements were possible in crust as young as 100,000 years. Beginning with a field of low heat flow approximately 3 km south of the rift axis, a smoothly alternating sequence of zones of high and low heat flow with distance from the axis can be observed. The array of the heat flow zones is essentially parallel to the rift axis, although some deviation from this pattern is visible with increasing distance from the

¹Department of Geological Sciences, University of Rochester, Rochester, New York 14627.

²Exxon Production Research Co., Houston, Texas 77001.

³Woods Hole Oceanographic Institution, Woods Hole, Massachusetts 02543.

⁴Department of Geosciences, Pennsylvania State University, University Park, Pennsylvania 16802.

Copyright 1983 by the American Geophysical Union.

Paper number 2B1614.

0148-0227/83/002B-1614\$05.00

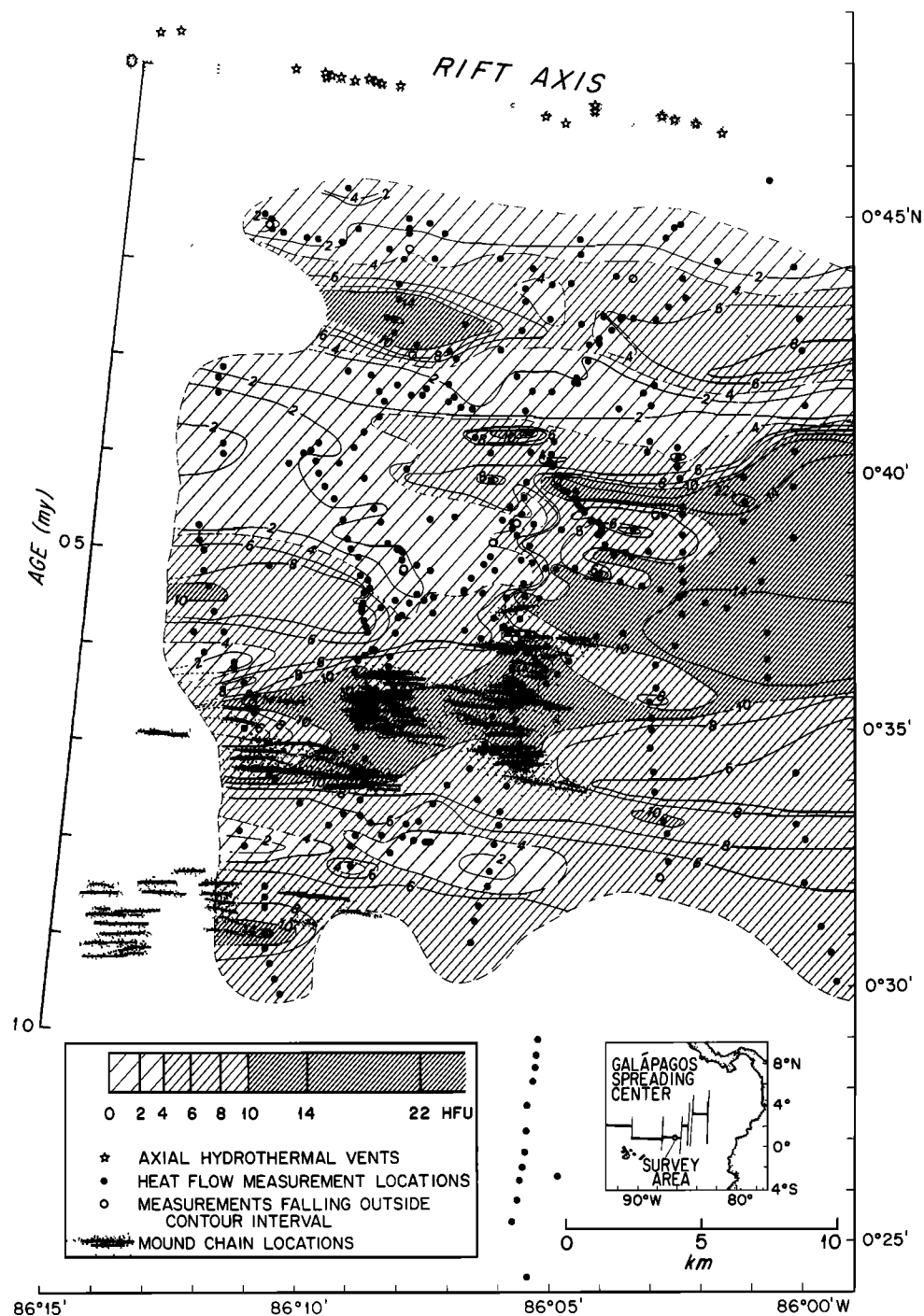


Fig. 1. Heat flow distribution at the south flank of the Galapagos Spreading Center, 86°W [from Green et al., 1981].

rift axis. The highest heat flow values were observed in zones characterized by the presence of hydrothermal mounds. These mounds, which stand up to 20 m above the seafloor, are composed principally of iron silicates and manganese oxides. They occur in chains approximately parallel to the ridge axis and are usually associated with fractures or faults in the crustal rocks [Williams et al., 1979]. Mounds were found in two distinct fields in the southwestern part of the survey area, separated

by a gap of about 5 km. The existence of hydrothermal mounds in the eastern part of the area is uncertain because of a lack of near-bottom echo sounding or sonar data [Klitgord and Mudie, 1974]. While a local correlation seems to exist between the topography and the heat flow distribution (i.e., the heat flow on the elevated parts of scarps is, in general, higher than on the depressed parts), the overall distribution of heat flow in the survey area is apparently independent of the topography [Green

et al., 1981], consistent with recent physical modeling of the topographic control of fluid convection [Hartline and Lister, 1981].

The main characteristics of the heat flow field relevant to the numerical modeling are the following:

1. The areal pattern revealed by 443 heat flow stations is roughly two dimensional. Fields characterized by either high or low heat flow are, in general, parallel to the ridge axis. We can therefore construct a two dimensional diagram of the heat flow variation with age or increasing distance from the ridge axis. Figure 2 shows the mean heat flow with distance south of the ridge axis.

2. All the active and inactive hydrothermal vents were found at the ridge axis.

3. The heat flow varies relatively smoothly over the area with peaks at distances of 6, 14, 22, and 30 km from the ridge axis. The mean conductive heat flow in the region increases strongly within the first 14 km from the ridge crest and averages close to that predicted by plate models from about 18-32 km. There is a slight increase in the heat flow going from west to east, i.e., parallel to the ridge axis.

4. The mean heat flow averaged over the entire survey area (not including the ridge axis)

is 305 mW m^{-2} which is approximately 40% of that predicted by models of conductively cooling plates.

5. There exist at least two distinct fields of hydrothermal mounds, both of which are associated with high heat flow. The area separating these two fields does not have mounds and is characterized by low heat flow.

6. Locally elevated heat flow occurs consistently on the elevated side of scarps paralleling the axis of spreading, with depressed heat flux at the base of scarps. The regional distribution of heat flow, however, is not correlated with the topography.

The Numerical Model

The numerical model used in our calculations is based on equations for flow through porous media. The model was first developed by Cathles [1977] and then adapted for the situation at mid-ocean ridges by Fehn and Cathles [1979] and Green [1980]. The basic equations are Darcy's law:

$$-\nabla p + \rho \underline{g} - \frac{\nu}{k} \underline{q} = 0 \quad (1)$$

balance of mass

$$\nabla \cdot \underline{q} = 0 \quad (2)$$

and balance of heat

$$\rho_m c_m \frac{\partial T}{\partial t} = -\nabla \cdot \underline{q} c_f T + K_m \nabla^2 T - \rho_m c_m \underline{v}_s \cdot \nabla T \quad (3)$$

where c_f is the specific heat of fluid ($c_f = H/T$, H is the enthalpy), c_m specific heat of fluid saturated rock ($0.2 \text{ cal/g } ^\circ\text{C}$), g gravitational field strength (980 cm/s^2), k permeability, K_m thermal conductivity of fluid-saturated rock ($6 \times 10^{-3} \text{ cal/}^\circ\text{C cm s}$), p pressure, q mass flux, v_s half spreading rate (cm/yr), ν kinematic viscosity, ρ_m density of fluid-saturated rock (2.7 g/cm^3), and ρ density of fluid. This system of equations is solved by standard finite difference techniques [e.g., Carnahan et al., 1969]. For the calculations here we chose a constant grid spacing with 60 grid points in the horizontal direction and 14 grid points in the vertical direction; i.e., the distance between grid points is 0.4 km or less in our models. Instead of the Boussinesque approximation for the solution of the equations we used the temperature- and pressure-dependent properties (enthalpy, density, and heat capacity) of pure water in our calculations. In the above equations, temperatures of matrix and fluid are identical, i.e., it is assumed that fluid and rock are in local thermal equilibrium throughout the region. This assumption is justified because of the fluid velocities calculated, except perhaps directly at the discharge areas in the rift valley. The observation that the heat flow distribution is roughly parallel to the ridge axis suggests that the spreading axis acts as a center of symmetry and determines the geometry of at least the circulation close to the axis. We therefore assume in our models two-dimensional fluid flow normal to the ridge axis. Because the

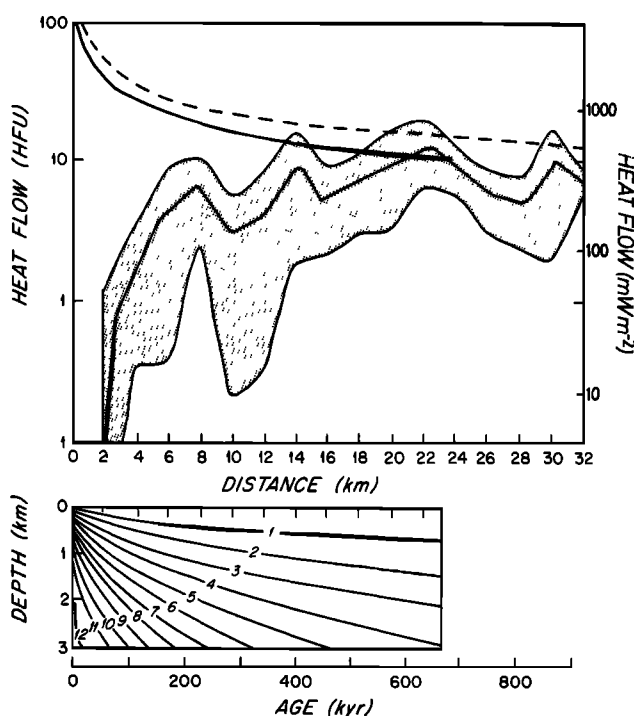


Fig. 2. Mean heat flow \pm one standard deviation (stippled area) versus distance from the ridge axis at the Galapagos Spreading Center. The data were averaged over nonoverlapping 2-km-wide strips parallel to the ridge axis. The observed heat flow distribution is compared to the empirical $11.3/\sqrt{t}$ relation (dashed curve; Parsons and Sclater [1977]) and to the heat flow produced by a model (shown in the lower part of the diagram) of a conductively cooling plate (solid curve). The difference between the numerical model and empirical curves arises from the use of material parameters appropriate for young oceanic crust.

heat input at the ridge axis and from below is thought to be the primary driving force of the convective system, and the influence of the topography on the flow distribution is probably secondary [Hartline and Lister, 1981], we used a flat topography for our models. Although most of the area is covered by sediments, we assume here that they are sufficiently thin and unsettled to not impede significantly the movement of water into the oceanic crust. This assumption seems acceptable in view of recent investigations of pore water movement in young marine sediments [Maris and Bender, 1982; Sayles and Jenkins, 1982] which suggest that flow rates there are of the same magnitude as those calculated in our models.

Boundary and Initial Conditions

The choice of boundary and initial conditions is an integral part of numerical modeling and can strongly influence the results of the calculations. All of our models with the exception of the high permeability models (surface permeability $5 \times 10^{-14} \text{ m}^2$) were started from a conductive solution for the temperature distribution in the domain. In the case of high surface permeability we used the solution for a low permeability model as initial condition. Because we computed all of our models until quasi-steady state in the domain was reached, the choice of initial conditions did not significantly affect the results of our models. As a test, we ran models with different initial temperature distributions (e.g., a cold, $T=0$ initial temperature throughout the domain or a temperature distribution linearly increasing with depth). While the evolution of the fluid flow and of the temperature distribution within the domain varied markedly, all models with an identical permeability distribution reached similar quasi-steady state solutions regardless of the initial conditions. As criteria for reaching the quasi-steady state, we used the average temperature in the domain. We use the term quasi-steady state here because although the average temperature and the total mass flux approach a constant value with time, as demonstrated in Figure 3 for the average temperature of various models, individual convection cells continue to move within the domain even after the quasi-steady state has been reached. We will take up this observation later when the results of the individual models are being discussed. As shown in Figure 3, large amounts of heat (and associated fluid) are transferred out of the domain during the transitory stages of the various models. We are not interested in this initial flow of heat and fluid for it would occur only if fluid convection were to change because of a significant increase in permeability or if a jumping spreading center were to force flow in older crust.

In contrast to the initial conditions, boundary conditions have a strong influence on the results of our models. Fluid flow was assumed to have free discharge only through the surface of the domain, i.e., through the seafloor. Using the ridge axis as symmetry plane and the lower boundary as limit of fluid flow penetration, we kept these boundaries im-

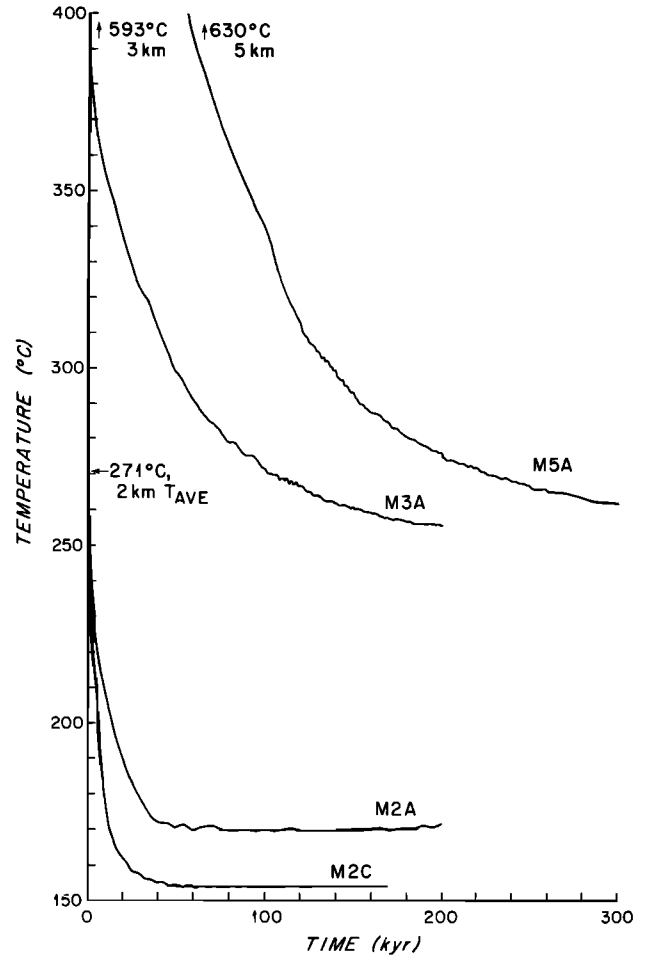


Fig. 3. Evolution of average temperatures in the domain after the onset of convection. The time necessary to reach quasi-steady state depends on the depth of the circulation (see Table 1 for model parameters).

permeable in the calculations. The vertical boundary opposite to the ridge axis could have been kept either permeable or impermeable; in either case, flow at this boundary is predetermined. The influence of this boundary on the flow distribution, however, is probably small, as long as the width of the domain is large compared to the width of a single convection cell. We chose an impermeable outer boundary. The thermal boundary conditions reflect our assumptions of the way hydrothermal convection is driven in young oceanic crust. The boundary at the ridge axis is modeled following a suggestion by Oldenburg [1975].

$$-K_m \frac{\partial T}{\partial x} = \rho_m v_s (L + (T_m - T_f(t,z)) c_m) \quad (4)$$

where L is the latent heat of fusion ($= 100 \text{ cal/g}$), T_m is the intrusion temperature (1200°C), and T_f is the boundary temperature calculated at the end of the previous time step. This boundary condition assumes a continuous spreading process at the ridge axis. The differences between boundary conditions for continuous and episodic spreading processes were

studied in a previous investigation [Fehn and Cathles, 1979]. Both boundary conditions resulted in comparable heat and flow distributions in the domain of interest. It was concluded then that a continuous heat input at the ridge axis was a good representation of the spreading process even at low spreading rates. Because the intrusion process is not directly modeled here but only its average effect, we felt justified in using this boundary condition for the ridge axis.

The boundary condition for the lower limit of the domain was derived from a conductive model for the oceanic crust underlying the hydrothermal layer. The temperature as a function of distance from the axis and depth within the plate resulting from a balance of horizontal advection and vertical conduction of heat to an isothermal upper surface at $T=0$ is given by Lister [1972]:

$$T(x,z) = T_M \operatorname{erf}(z(4\kappa x/v_s)^{-1/2}) \quad (5)$$

where T_M is the initial temperature and κ is the thermal diffusivity. The derivative of this function evaluated at the base of the hydrothermal layer was used as the heat flux into the hydrothermal layer:

$$Q(x,H) = (KT_M/(\pi\kappa x/v_s)^{1/2}) \exp(-H^2/(4\kappa x/v_s)) \quad (6)$$

Because the injected material at the ridge axis is initially isothermal, the heat flow into the base of the layer is zero at the origin. The heat flow goes through a maximum before it approaches a $(t)^{-1/2}$ distribution. The location and the sharpness of the maximum depends on the thickness of the hydrothermal layer. In Figure 4, the heat flow distribution on the base of the hydrothermal layer is compared for three

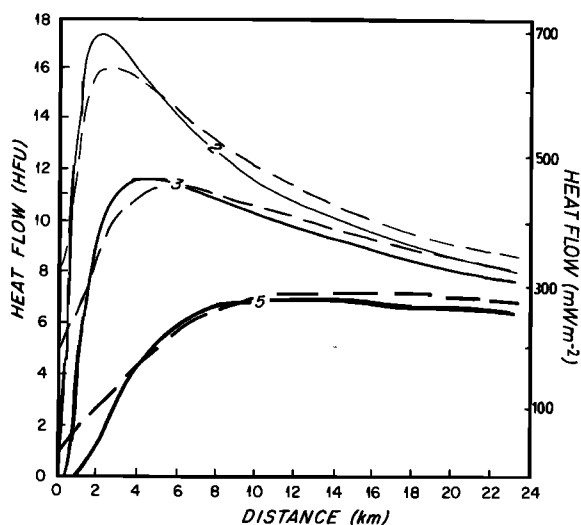


Fig. 4. Solid curves, heat flow into the base of the models versus distance. Dashed lines, the Davis and Lister [1974] series solution heat flux, evaluated at the depth of the models using the same thermal parameters as in the numerical model.

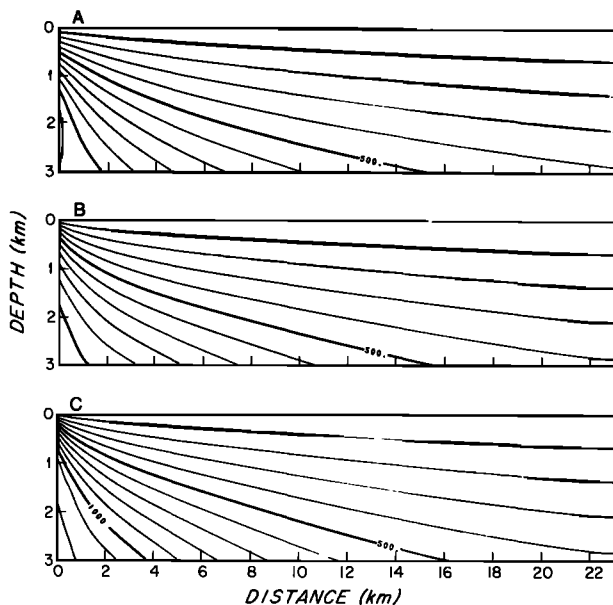


Fig. 5. Equilibrium temperature distribution for conductively cooling crust. (a) Davis and Lister [1974] series solution using an 80-km plate, with spreading velocity of 3.5 cm/yr, evaluated over the upper 3 km. (b) Numerical model solution neglecting latent heat. (c) Numerical model solution with 100 cal/g latent heat, advected in with the plate.

different thicknesses. These distributions are in good agreement with those calculated on the basis of the model developed by Davis and Lister [1974], which also incorporates lateral conduction within the crust. The temperature distribution within the top 3 km of conductively cooling crust is shown in Figure 5. Again, good agreement can be observed between the results of the finite difference model and the series solution model by Davis and Lister [1974]. Temperatures above 1000°C within the upper 2 km occur in these conductively cooling models, which would allow the presence of shallow magma chambers at these moderate ($v_s = 3.5$ cm/yr) spreading rates [Sleep, 1975].

Because lateral conduction apparently has only a small effect on the temperature distribution in the oceanic crust, we felt justified in assuming an insulating boundary away from the ridge axis. This choice of a thermal boundary condition also complies with the fluid flow condition, which prevents convective heat transport through this boundary. It should be noted, however, that because of the plate motion, heat still leaves the domain through this boundary.

At the surface of the domain we assumed a constant temperature of $T = 0^\circ\text{C}$. This boundary condition formally requires all heat flow at the surface to be conductive, although in reality this total heat flow may be partly conductive and partly convective. Except for hot vents at the ridge axis, the contribution of convective heat losses through the surface probably is small at the velocities calculated in our or similar models [e.g., Ribando et al., 1976]. As an approximation, we evaluate the total heat flow and the conductive heat flow at the first grid point below the surface.

Total heat flow at this depth is a good estimate of the total heat flow through the surface, while the conductive contribution gives a useful measure of the conductive heat flow to be expected in these areas.

Discussion of the Approach

As in any kind of modeling, the limitations of the approach have to be kept in mind in order to make proper use of the results. We use here a two-dimensional model where the fluid flow is driven by the heat input from the ridge axis and from the cooling crust underlying the hydrothermal layer. Within the hydrothermal layer we assume that fluid flow is governed by the theory of flow through porous media, i.e., that a predetermined bulk permeability distribution within the oceanic crust is a satisfactory representation of the actual situation. It follows from these assumptions that the flow distribution in our models primarily depends on the prescribed heat input and on the permeability distribution. Other factors, such as topography, local inhomogeneities in the permeability, and a thin, patchy sediment cover are then influences of secondary order which we do not attempt to model. By comparing the results of our models to the observed heat flow distribution, we can determine whether or not our assumption can comply with the actual convection mechanism. It is clear, however, that due to the complexity of the problem, we cannot rule out other possible mechanisms for the hydrothermal convection, even if our results are in good agreement with the observed data.

A major problem for the understanding of hydrothermal convection is the question of permeability in young oceanic crust. Estimates of the average permeability and of the permeability distribution vary widely. An apparent discrepancy exists between the permeabilities used in model calculations, which are typically around 10^{-15} m^2 [e.g., Ribando et al., 1976; Fehn and Cathles, 1979], and those determined for young oceanic crust. Anderson and Zoback [1982] estimate a minimum value of $4\text{--}40 \times 10^{-15} \text{ m}^2$ obtained in in situ experiments at the Costa Rica Rift. Other authors [e.g., Johnson, 1980] arrive on the basis of fissure distribution in drill cores at permeabilities several orders of magnitude higher than the model permeabilities. It should be kept in mind, however, that the measured permeabilities so far all come from the top 200 m of oceanic crust, while the model calculations cover the entire hydrothermal layer up to depths of 5 km. It seems quite likely that permeability decreases with increasing depth, although the relation between depth and permeability is not known. In most of our models we assume an exponential decrease of permeability with depth. The permeability range tested in our models expands the range to somewhat higher model permeabilities so that an overlap exists with the experimentally determined range. Based on our calculations, we believe that the permeability range used in our models is a fair representation of the average permeability of the oceanic crust, which does not, however, exclude the possibility that permeabilities exist locally which may be several

orders of magnitude higher than those used in our models.

Model Calculations

The free parameters which remain for the modeling after the heat input into the oceanic crust is defined by the boundary conditions are the permeability distribution within the hydrothermal layer and the depth of penetration of the hydrothermal convection. The permeability distributions and the penetration depths used in our models are listed in Table 1. We computed models for penetration depths between 2 and 5 km with surface permeabilities varying between 50 and $0.5 \times 10^{-15} \text{ m}^2$. The permeability was assumed to be isotropic and, in most cases, to decrease exponentially with depth. As mentioned earlier, no effort was made to model the influence of the topography or of the thin sediment cover because both of these influences were considered to be secondary here. For reasons of comparison we calculated models with uniform permeability (models M2D and M2E), with a different lower boundary condition (model M2B), as well as one using the Boussinesque approximation (model M2F) instead of the temperature- and pressure-dependent thermal properties of the circulating fluid. Model results for various parameters are summarized in Table 2. Rayleigh numbers are usually calculated as a measure for the vigor of flow in a convection cell. In our case, however, we are not dealing with Rayleigh-Benard convection but with flow which is forced essentially by lateral temperature gradients due to the intrusion process at the ridge axis. Furthermore, the thermodynamic properties of water depend strongly on temperature and pressure and vary significantly in lateral and vertical direction throughout the domain. For these reasons, we felt that Rayleigh numbers were only of questionable use for our models.

In Figure 6, the temperature and flow distributions are compared for four of our models. In all of the models a strong convection cell has developed, associated with the intrusion process at the ridge axis (left boundary). Convection penetrates either to the impermeable lower boundary, as in the 2-km-deep models, or until the permeability, which in all of these models decreases exponentially with depth, falls below about $0.05 \times 10^{-15} \text{ m}^2$. Secondary cells develop away from the ridge axis in all models, the number of which depends strongly on the permeability distribution in the domain. In model M2A, which has a surface permeability of $5 \times 10^{-15} \text{ m}^2$, convection dies out very quickly; only one secondary zone of upwelling flow is created. If the permeability is increased by a factor of 10, as in model M2C, a sequence of regularly spaced convection cells develops, and convection continues throughout the domain. An increase in the depth of penetration has a similar effect, as long as the added layer has a sufficiently high ($>0.05 \times 10^{-15} \text{ m}^2$) permeability. Therefore, only little difference exists in the convection pattern of models M2A and M3A, which both have the same surface permeability of $5 \times 10^{-15} \text{ m}^2$ and an identical rate of permeability decrease with depth (i.e., the added layer between 2 and 3 km is essentially cooled by conduction).

TABLE 1. Model Parameters

Model	Depth of Penetration, km	Surface Permeability, 10^{-15} m^2	Bottom Permeability, 10^{-15} m^2	Permeability Distribution	Remarks
M2A	2	5.0	0.05	exp. decreasing	
M2B	2	5.0	0.05	exp. decreasing	Lower boundary isothermal at 333°C corresponding to a constant heat flux of 420 mW m^{-2}
M2C	2	50.0	0.05	exp. decreasing	
M2c	2				Conductive solution
M2D	2	5.0	5.0	constant	
M2E	2	0.5	0.5	constant	
M2F	2	50.0	0.5	exp. decreasing	Constant thermal properties for water; Boussinesque approximation
M3A	3	5.0	0.005	exp. decreasing	
M3c	3				Conductive solution
M5A	5	5.0	0.005	exp. decreasing	
M5c	5				Conductive solution

TABLE 2. Model Results for Maximum Stream Function, Maximum Temperature, Average Temperature, Total Mass Flux, and Total Heat Flux

Model	$\psi_{\max} \pm \text{s.d.}$	$T_{\max} \pm \text{s.d.},$ °C	$T_{\text{ave}} \pm \text{s.d.},$ °C	Mass Flux $\pm \text{s.d.},$ 10 ⁶ g/yr/cm	Heat Flux $\pm \text{s.d.},$ W/cm
M2A	10.09 \pm 3.59	529.00 \pm 23.3	171.50 \pm 0.50	1.896 \pm 0.501	159.5 \pm 28.9
M2B	8.91 \pm 3.40	458.80 \pm 19.68	153.59 \pm 0.25	1.398 \pm 0.433	144.2 \pm 28.1
M2C	23.13 \pm 2.84	327.89 \pm 1.36	91.92 \pm 0.02	8.041 \pm 0.362	164.7 \pm 12.1
M2D	16.90 \pm 0.19	303.57 \pm 6.811	75.42 \pm 2.75	6.261 \pm 0.381	171.3 \pm 7.6
M2E*	8.09 \pm 0.36	487.56 \pm 38.34	153.80 \pm 0.16	1.922 \pm 0.070	174.1 \pm 5.4
M2F	14.50 \pm 0.00	638.80 \pm 0.00	132.36 \pm 0.05	7.560 \pm 0.052	168.6 \pm 0.3
M3A	10.57 \pm 2.91	(1200.)	256.20 \pm 0.20	2.138 \pm 0.564	186.6 \pm 36.0
M5A	16.24 \pm 2.66	(1200.)	262.06 \pm 0.29	3.484 \pm 0.482	214.1 \pm 33.5

*Model M2E had only 11 grid points vertically, leading to largest variation in T_{\max} .

Convection in the 5-km-deep model M5A, however, which has the same surface permeability but an increased e-folding depth, is much more vigorous than in model M2A and continues throughout the domain.

The strong convection close to the ridge axis observed in all of these models causes a sharp decrease in temperatures in the axial region as compared with the conductive model (see Figure 5). Even in the region with upwelling flow, temperatures are, in general, lower than in the conductive case. Temperatures in the rest of the domain reflect the presence of convection; i.e., they are higher in regions with upwelling than with downwelling flow. The average temperatures, however, remain rather constant throughout the domain after the initial cooling in the axial region. In most cases a small increase in average temperatures between the axial cell and the second cell can be observed. This observation indicates that convection associated with the axial intrusion process removes in these cases all the excess heat from the axial intrusions. Therefore, the fluid flow in the rest of the domain is driven from the heat input coming through the lower boundary and serves mainly to prevent reheating of the oceanic crust.

In Figure 7, the heat flow distributions associated with these four models are shown. As mentioned earlier, heat flow is evaluated at the first grid point below the surface. For each model, total heat flow which consists of the conductive and convective contribution, as well as the conductive heat flow are given. The heat flow distributions are compared to the heat flow calculated from the conductive solution. In all cases, the heat flow distribution has a sharp maximum at the ridge axis associated with the strong axial convection cell. A zone of heat flow depressed below the conductive values follows, the width of which depends on the per-

meability distribution. While for models M2A and M3A the heat flow quickly approaches that of the conductive case, in the other two models the calculated heat flow continues to oscillate around the conductive heat flow distribution throughout the domain.

In all models, upwelling flow is more concentrated than downwelling flow. As a consequence, zones with heat flow lower than predicted are significantly broader than those with higher heat flow, a result which is in good agreement with the observations at the Galapagos Spreading Center and at other active rifts [e.g., Williams et al., 1977]. This effect occurs here in the absence of fractures or other zones of high permeability, which can serve to concentrate further the upwelling flow [Fehn and Cathles, 1979]. The main reason for this effect is the temperature dependence of the thermal properties of water. If we use the Boussinesque approximation in our calculations (model M2F), i.e., constant thermal properties and a linear expansion coefficient instead of the real temperature and pressure dependence of water, the resulting flow distribution (Figure 8) shows zones of upwelling flow covering as much area as the zones of downwelling flow. A comparison between models M2C and M2F, which have the same permeability distribution, also shows that maximum and average temperatures are significantly lower in model M2C than in model M2F (see Table 2), while mass fluxes are almost identical in both models. As was found in previous investigations [e.g., Cathles, 1977], the effectiveness of convective cooling is significantly underestimated if the temperature dependence of the thermal properties of water is not taken into account.

Although the average temperatures within the domain approached a steady state value after some time, we found that in all of our models the circulation cells off-axis were not fixed

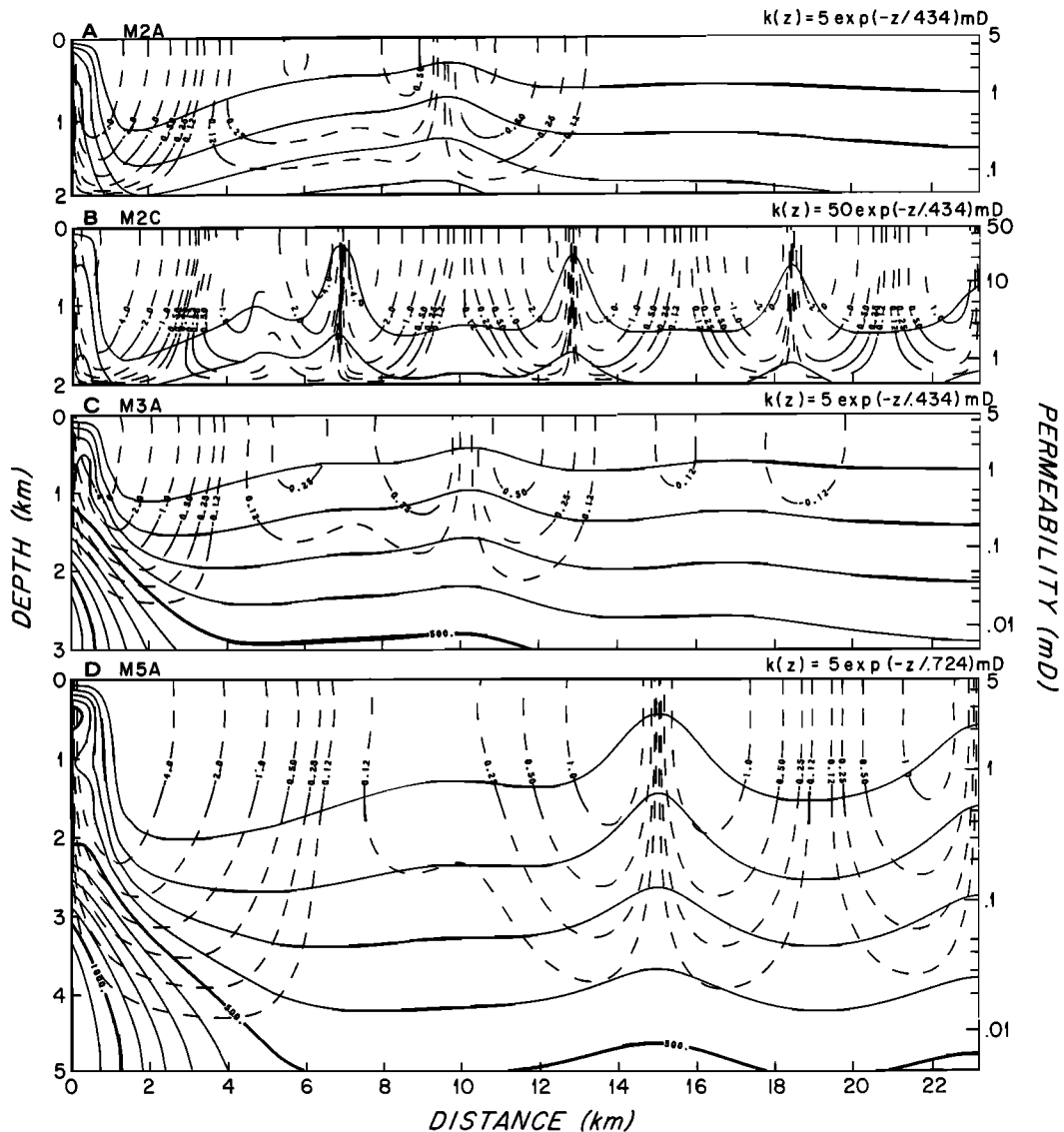


Fig. 6. Model stream functions (dashed lines) and isotherms (solid lines) for four models. The cross sections show the situation just prior to the formation of new zones of upwelling flow near the axis. The dimensionless stream function interval is variable in order to show the structure of the flow in regions of widely varying intensity. The intervals increase by factors of 2 from 0.125. Isotherms are given in 100°C intervals with the 500°C and 1000°C isotherms emphasized. Vertical exaggeration is 2 x. Permeabilities in millidarcies (1 mDarcy = 10^{-15} m²).

with respect to the ridge axis but migrated with the moving plate. In Figure 9, the evolution of the cell distribution within the domain is demonstrated for model M2C. The sequence starts after quasi-steady state circulation was obtained. While the axial cell and the second zone of upwelling flow remains constant with respect to the ridge axis, the third zone of upwelling moves away from the ridge axis. As the distance between the two upwelling zones increases, the intensity of the downwelling zone decreases and allows a local zone of conductive reheating midway between the two zones of upwelling. This disturbance in the isotherms causes the initiation of a set of small convection cells which eventually reach the surface. This new zone of upwelling flow

remains relatively stationary until the distance to the next zone of upwelling corresponds to the natural wavelength of the model with the given permeability distribution and depth. Then the zone of upwelling starts to migrate together with the other convection cells, and the process starts over again.

In other cases, the generation of new convection cells took place in the broad zone of downwelling flow adjacent to the axial cell. In Figure 10 the migration of cells is demonstrated for model M2D, a model with constant permeability. Each point gives the location of a zone of upwelling at a given time. In general, the points lie on lines parallel to the heavy dashed line, which indicates the plate velocity. The cells thus move at plate

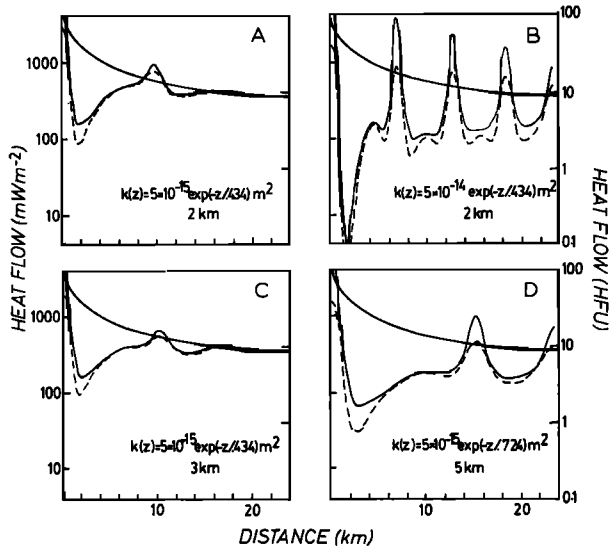


Fig. 7. Heat flow for the models shown in Figure 6. Total heat flow (solid lines) consists of the conductive heat flow (dashed lines) and the heat transported by the fluid flow. The heat flow profiles from the corresponding conductive models are shown for reference.

velocity as long as their motion is not disturbed by the generation of new convection cells. In this case, a pair of cells is created at around 120×10^3 years. The dis-

tance to the next zone of upwelling, however, is too small for stability, so that the two zones join after 50×10^3 years, forming a broad zone of upwelling for some time. The process will be repeated at 200×10^3 years, when the cells have moved sufficiently away from the ridge axis.

The results of our models have several features in common, which can be summarized as follows:

1. The convection cell associated with the intrusion process at the ridge axis has the strongest convection. Convective heat transfer from this cell is sufficient to remove all the excess heat from the axial intrusion process.
2. A series of convection cells develops off-axis. They are driven by the heat input from below and prevent the reheating of the oceanic crust. Spacing of these secondary cells depends on the permeability distribution in the domain and on the vigor of the axial convection.
3. Due to the temperature dependence of the thermal properties of water, upwelling flow is significantly more concentrated than downwelling flow even in the absence of fractures or other zones of high permeability.
4. Most cells off-axis follow the plate motion. Because the axial cell is fixed by the intrusion process at the spreading center, a zone exists where the spacing between cells is unstable and where new convection cells are created.
5. Hydrothermal convection causes a significant decrease in average temperatures as

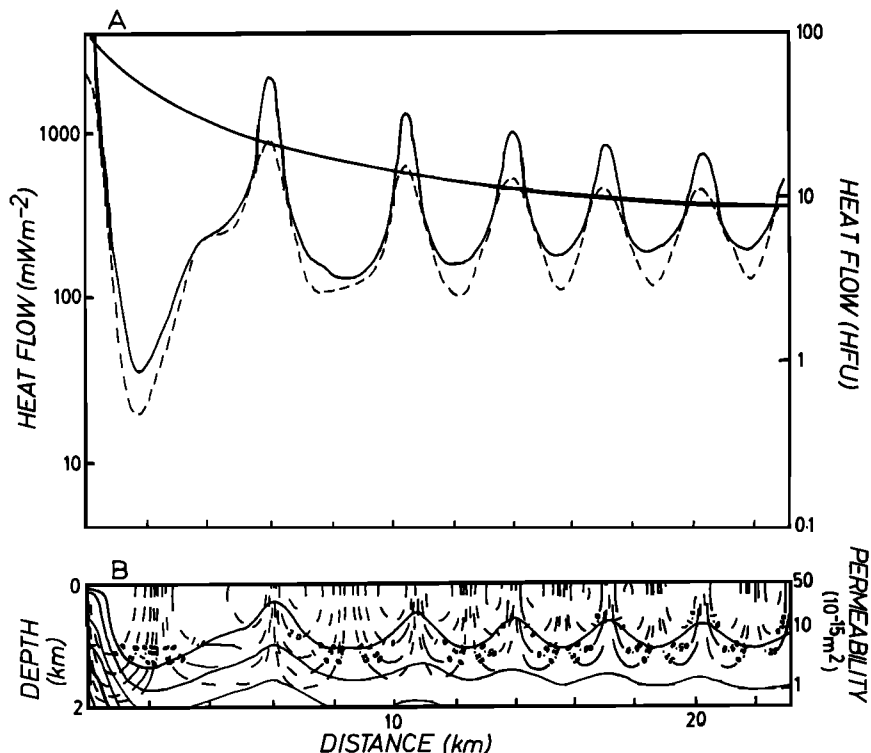


Fig. 8. Heat flow and cross section for model M2F. Constant thermal expansion coefficient of $10^{-3} (\text{C})^{-1}$, heat capacity $1.0 \text{ cal g}^{-1} (\text{C})^{-1}$, and viscosity ($10^{-3} \text{ cm}^2 \text{ s}^{-1}$) were used. Note the more symmetrical distribution of zones of upwelling and downwelling fluid flow as compared to the models where variation of thermal properties of water is taken into account.

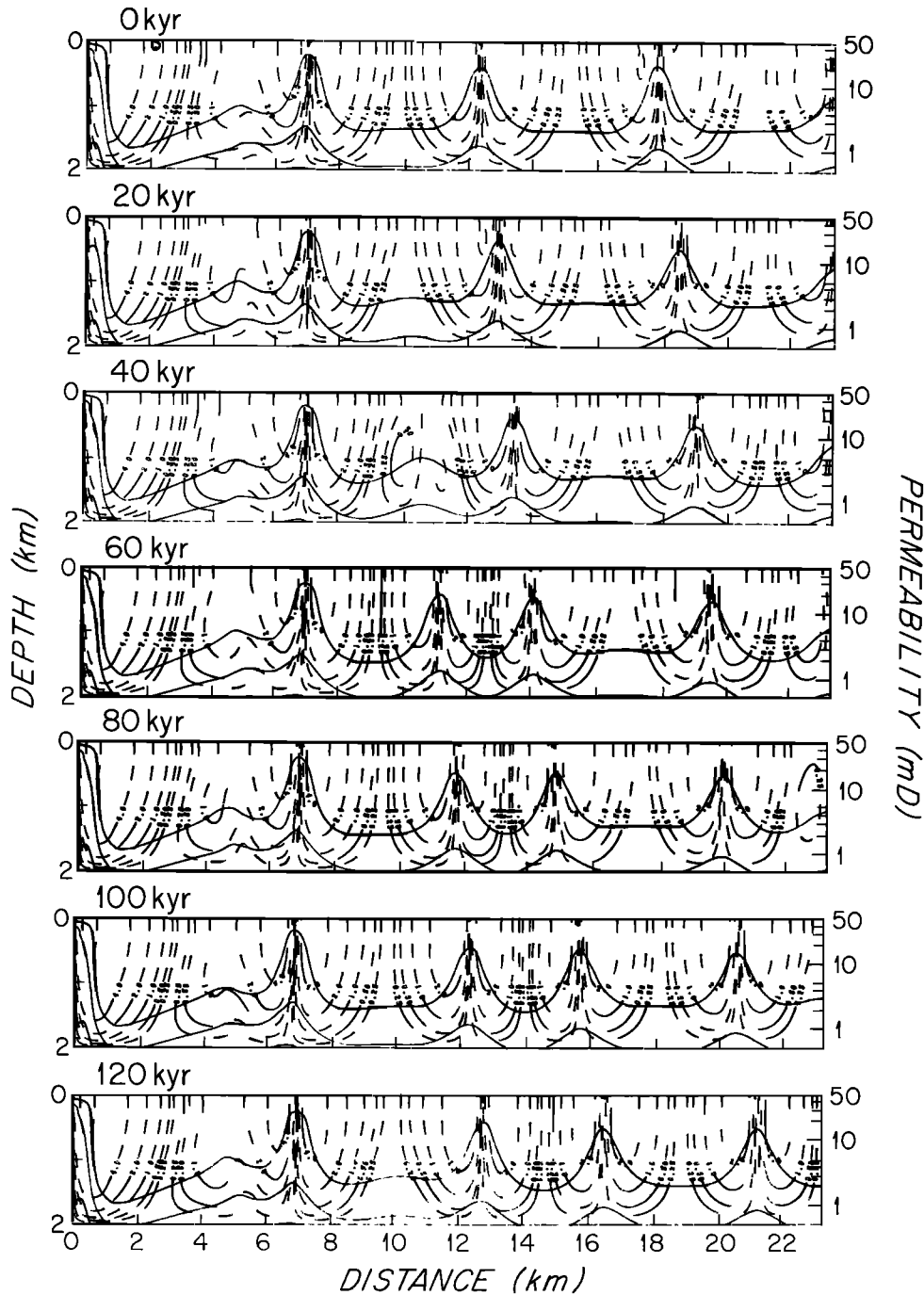


Fig. 9. Time evolution of model M2C, after equilibrium circulation was obtained. (1 mDarcy = 10^{-15} m²).

compared to the conductive case. The amount of cooling depends on the permeability distribution in the crust. Temperatures in the convection cells are below 300°C except for some regions at the ridge axis.

Comparison of Model Results to Observed Heat Flow Distribution

The heat flow distribution predicted by our models can now be compared to the observed heat flow distribution at the Galapagos Spreading Center. In several of our models, such as M2A

and M3A, convection is essentially limited to the region immediately adjacent to the ridge axis, and consequently, heat flow approaches that of the conductive solution within the region of investigation. Because the cyclical variation in the observed heat flow field continues beyond an age of 1 m.y., permeabilities in the models were either too low or decayed too quickly with depth to match the observation. On the other hand, in a model with significantly higher permeability, model M2C, but shallow depth of penetration, the spacing between zones of upwelling, i.e., high heat flow zones, seems

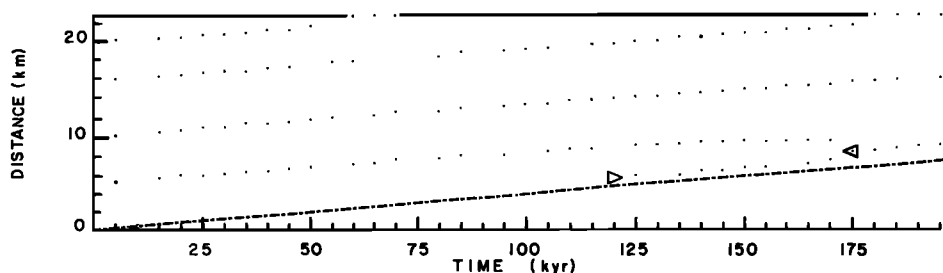


Fig. 10. Migration of cells with time in model M2D. The dashed line marks the plate movement due to the spreading process. Each dot indicates the location of a zone of upwelling fluid flow at intervals of 5000 years. The upwelling forced by the intrusion process at the ridge axis is fixed and is not shown. The off-axis upwellings parallel the plate motion, maintaining the same relative separation. The open triangle at 120,000 years indicates the appearance of a new zone of upwelling. Under the influence of this new upwelling zone, the leading upwelling zone stops migrating, and the two zones merge at 175,000 years.

to be too small compared to the actual heat flow distribution. In Figure 11, the observed heat flow distribution is superimposed on the heat flow calculated for model M5A, which has a surface permeability of $5 \times 10^{-15} \text{ m}^2$ exponentially decreasing to $0.05 \times 10^{-15} \text{ m}^2$ over the penetration depth of 5 km.

Several remarks are in order before the two sets of data can be compared meaningfully. As in the previous heat flow diagrams, total heat flow and conductive contribution are plotted, both evaluated at the first grid point in the domain. These two curves bracket the actual model heat flow at the surface. Because of the motion of the convection cells, zones of upwelling and the associated zones of high heat flow are not stationary. In addition to the heat flow distribution, which was calculated for a time of 250×10^3 years after the onset of convection, we also indicated the size and location of the heat flow maxima for 50×10^3 years before and after that time.

The observed and the calculated heat flow

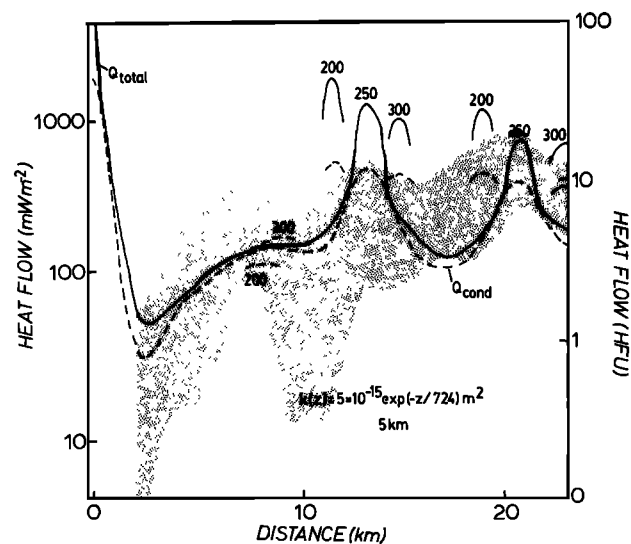


Fig. 11. Observed heat flow variation compared to the heat flow calculated in model M5A at three time steps.

distributions agree, in general, quite well, although the location of the first heat flow maxima does not seem to match so closely, which may indicate that the penetration depth near the ridge axis is shallower than the 5 km of the model. It is interesting to note that in this model the first heat flow maximum away from the ridge axis is not caused by upwelling convection but by the lack of downwelling flow, which allows for conductive reheating in this region. Because of the motion of the cells, the actual location of the upwelling zones off-axis is less meaningful than the spacing between them. The wavelength for the heat flow distribution calculated for this model here seems to be quite compatible with the observation, especially if the continuation of the heat flow field is also taken into account (see Figure 2). Except for the axial region, then, the permeability distribution and the penetration depth used in this model generate a heat flow distribution which is in apparent agreement with the observations. It would certainly be possible to construct models which match the observed heat flow distribution more closely, particularly if more complicated permeability distributions would be used. We feel, however, that the nonstationary behavior of the cells off-axis coupled with the general lack of knowledge of the permeability distribution in the oceanic crust would give a false sense of accuracy of such models.

Discussion

In spite of the many simplifying assumptions necessary in models of this kind, the results of our calculations can be useful for the understanding of hydrothermal convection at mid-ocean ridges. It seems possible to generate model heat flow distributions which are quite compatible with the observed heat flow field. It is thus possible that at least the general features of hydrothermal convection associated with the intrusion process at mid-ocean ridges are described by simple geometrical models of porous media flow. According to this approach, the primary cause for a heat flow distribution as observed at the Galapagos Spreading Center is the input of heat from the intrusion process at the

ridge axis and from the cooling crust underlying the hydrothermal layer. The fluid flow distribution is governed by the permeability distribution within the hydrothermal layer. The models suggest that the average permeability of the upper layers of the oceanic crust is of the order of 10^{-15} m^2 and that the thickness of the hydrothermal layer is between 2 and 5 km. It seems likely from a comparison between calculated and observed heat flow distributions that the penetration depth of hydrothermal convection increases with increasing distance from the ridge axis (see Figure 11).

An important result of our models is that convection cells are not fixed with respect to the spreading center but move with the moving plate. As a consequence, individual segments of oceanic crust experience, once they have left the immediate vicinity of the spreading center, either continuous upward or downward flow. Because the influence of hydrothermal convection on the geochemistry of the oceanic crust depends strongly on temperature and the ratio of water to rock [e.g., Bischoff and Dickson, 1975; Mottl, 1982], significant geochemical differences should be observable between zones of continuous upward or downward flow. It would be interesting to test this consequence in a few closely spaced drill cores over areas where heat flow indicates differences in the flow direction.

There is, perhaps, some indirect evidence that convection cells indeed move with the plate. In the Galapagos area, the fields of hydrothermal mounds are associated with high heat flow zones. The gap between the two fields, which is characterized by low heat flow, apparently does not contain hydrothermal mounds. It seems conceivable that the mound fields are expressions of zones of upwelling flow which are separated by zones of downwelling flow, all of which move away from the ridge axis, keeping the distance originally established by the convection cells. In this context, it is also interesting to note the absence of mounds over the first zone of high heat flow. It could be that the crust there is still too young for the creation of visible mounds or that upwelling flow does not necessarily form hydrothermal mounds. On the other hand, it seems possible that this first zone of high heat flow is not associated with upwelling flow but is caused by the absence of downwelling flow and the consequential reheating by conduction, as observed in some of our models. As mentioned earlier, in the eastern part of the survey region the bathymetric coverage is not sufficient to allow statements on the presence of hydrothermal mounds associated with the high heat flow zone in this region.

Although the presence of hydrothermal accumulations is reported from other parts of the mid-ocean ridge system, notably from the TAG hydrothermal field [Rona et al., 1976] and in the Gulf of Aden [Cann et al., 1977], neither of these observations is similar to the mounds in the Galapagos area. Data coverage in these and other areas is, however, not sufficient to allow conclusions as to whether hydrothermal mounds are a phenomenon peculiar to the Galapagos Spreading Center or whether they are of more widespread occurrence. Because the

mounds probably become covered with sediments as they move away from a ridge axis, it is also not known if they persist in older crust. An interesting observation in this connection is the presence of closely and regularly spaced small deposits of manganiferous chert in the Franciscan Assemblage. Crerar et al. [1982] suggested recently that these lenses were formed in a mid-ocean ridge setting. If so, these deposits can be interpreted as evidence for the movement of regularly spaced convection cells with a moving plate, where each zone of upwelling creates a small lens of manganese crust.

In our models the strongest convection occurred at the ridge axis. The heat transfer in this axial cell is in most of the cases so effective that all the heat associated with the axial intrusion process is removed by the axial cell. In some cases, convection in the axial cell was even strong enough to cause cooling of the adjacent segment of the oceanic crust. As a consequence, the less vigorous convection in the secondary convection cells was not sufficient to keep the crust at such a low temperature and a slow, but significant reheating of the crust was observable, which is in good agreement with the observed heat flow trend in the Galapagos area. The main result of convection in older crust is to keep the hydrothermal layer at temperatures typical for a given permeability distribution. Once hydrothermal convection stops, conductive reheating of the crust occurs, and the observed heat flow approaches the predicted heat flow, as shown in some of the models with low permeability. In the Galapagos area the average heat flow increases only very slightly with increasing distance from the ridge axis, i.e., hydrothermal convection continues throughout the region of investigation and only little reheating of the oceanic crust takes place. In other areas, such as the flanks of the Costa Rica Rift, an increase in heat flow is observed where the sediment thickness is sufficient to prevent hydrothermal convection [Langseth et al., 1981] or at least the loss of heat by advection through the seafloor. Reheating of the crust in this region seems to be a plausible explanation for this observation.

Temperatures within the convection cells are below 300°C with exception of the axial cell. The calculated temperature distribution at the axis is strongly dependent on details of the boundary conditions. These are not well determined and probably variable with location. It seems safe, however, to assume that distinct temperature differences exist between the first, the axial cell, and the other convection cells within the hydrothermal layer. If so, this result has important consequences for the geochemistry of the basalt-seawater interaction, which occurs in these convection cells. In the axial cell, temperatures are high ($>300^\circ\text{C}$) and fluid flow is rapid, but because of the relatively short residence time of the crust in the vicinity of the ridge axis, the seawater/rock ratio is low. Calculated water/rock ratios are around 1 for the axial cell. By the time the newly formed crustal material leaves the axial region, it has been substantially

cooled. Temperatures in the secondary cells therefore are significantly lower, and convection is slower than in the axial cell. Because, however, secondary cells move along with the plate, flow direction, once established, is constant in these cells, and consequently, high seawater/rock ratios can be achieved there. These results suggest that newly formed oceanic crust moves through very different hydrothermal systems, which have distinctly different effects on the geochemistry of the basalts. These differences occur as a result of the strong influence of temperatures and water/rock ratios on exchange reactions between seawater and basalt [e.g., Seyfried and Bischoff, 1977; Mottl, 1982].

This conclusion, that two geochemically different convection systems exist in young oceanic crust, was achieved here under the assumption that the spreading process at the ridge axis is continuous, but it probably is also applicable in the case of episodic spreading [e.g., Ballard and Van Andel, 1977; Ballard et al., 1982]. Calculations based on flow rates and temperatures in active vents [Macdonald et al., 1980] indicate that convective heat losses are more than sufficient to cool the intrusion at the ridge axis before the new crustal material leaves the axial region. In both cases, episodic intrusion and continuous spreading, convection in crust which has left the immediate vicinity of the ridge axis is practically independent of the intrusion process at the ridge axis. A similar result was found by Lister [1981], based on considerations of water penetration into cooling rock. He suggested that an 'active' system where water causes the opening of fractures in newly intruded crust be distinguished from a 'passive' system where water convects in an already existing permeability system in older crust. Because the process of water penetration into cooling rock is probably substantially faster than spreading rates, the 'active,' hot systems are associated only with the intrusion process at spreading centers regardless of spreading rates and mode of intrusion.

Although hydrothermal convection is sufficient to remove the excess heat of intruding magma at a spreading center, the cooling of the newly formed crust at the ridge axis is restricted essentially to the penetration depth of the seawater convection. Beyond the penetration depth, which probably ranges between 2 and 5 km, conductive cooling is the dominant mechanism for heat transfer. The heat flow highs in older crust, such as those associated with the mound fields in the Galapagos area, are evidence that substantial amounts of heat are transferred into the hydrothermal layer from the underlying cooling plate. The heat input into the hydrothermal layer from the cooling plate is strong enough to cause high heat flow and hydrothermal mounds at considerable distance from the ridge axis. On the other hand, the generally low temperatures in this layer caused by the convective heat losses make it unlikely that a shallow magma chamber could exist beyond the immediate vicinity of the ridge axis in the Galapagos area.

Total mass fluxes in our models range between

2 and 8×10^6 g/yr/cm of ridge (see Table 2) for the 23 km of the domain. Although a global estimate of the mass fluxes at mid-ocean ridges is beyond the scope of this paper, it is useful to compare our results to other estimates. If we extrapolate our results to a global estimate we arrive at mass fluxes between 2 and 8×10^{16} g/yr for the total ridge system. This result is somewhat lower than other estimates [e.g., Wolery and Sleep, 1976; Sleep and Wolery, 1978; Jenkins et al., 1978] which could have several reasons. First, the discrepancy between observed and predicted heat flow and the convection associated with it is not limited to the region we included in our calculations but apparently occurs in significantly older crust [e.g., Anderson et al., 1977, 1979]. Second, our boundary conditions produce a somewhat lower heat flow than the empirical heat flow distribution (e.g., $j = 11.3/\sqrt{t}$; Parsons and Slater [1977]). Finally, the gap between the observed and predicted heat flow is at least in the Galapagos region not as large as previously assumed [Green et al., 1981]. If these factors are taken into account, our results are in reasonably good agreement with mass flux estimates based on other assumptions.

Conclusion

The results of our calculations show that models based on the equations of flow through porous media and on defined heat input from the ridge axis and the cooling plate can produce heat flow distribution compatible with the observed heat flow field at the Galapagos Spreading Center. Important consequences of the model calculations are the following:

1. A system of convection cells develops in the oceanic crust, the size and extent of which depend on the permeability distribution in the oceanic crust. Our results suggest permeabilities in the range of 10^{-15} m² and penetration depths between 2 and 5 km for young oceanic crust.
2. Most of the convection cells move with the moving plate away from the ridge axis. Exceptions are the convection cells in the immediate vicinity of the ridge axis, which are fixed with respect to the spreading axis.
3. Temperatures within the hydrothermal layer are below 300°C except for the axial cell where higher temperatures are possible.
4. Newly formed oceanic crust is exposed to two distinctly different hydrothermal systems: first to the axial cell, characterized by high temperatures, high flow rates, and low water/rock ratios, and then to secondary cells, which have more moderate temperatures and flow rates but can reach very high water/rock ratios.

Acknowledgments. We acknowledge helpful comments from J. Whitehead, J. Crowe, B. Hartline, and an anonymous reviewer. The work was supported by funds from the NSF under grants OCE 77-28281 and 77-23470.

References

- Allmendinger, R. W., and F. Riis, The Galapagos Rift at 86° W, 1, Regional morphological and structural analysis,

- J. Geophys. Res.*, **84**, 5379-5389, 1979.
- Anderson, R. N., and M. D. Zoback, Permeability, underpressures, and convection in the oceanic crust near the Costa Rica rift, eastern Equatorial Pacific, *J. Geophys. Res.*, **87**, 2860-2868, 1982.
- Anderson, R. N., M. G. Langseth, and J. G. Sclater, The mechanisms of heat transfer through the floor of the Indian Ocean, *J. Geophys. Res.*, **82**, 3391-3409, 1977.
- Anderson, R. N., M. A. Hobart, and M. G. Langseth, Geothermal convection through oceanic crust and sediments in the Indian Ocean, *Science*, **204**, 828-832, 1979.
- Ballard, R. D., and T. H. Van Andel, Morphology and tectonics of the inner rift valley at lat. 36°50'N on the Mid-Atlantic Ridge, *Geol. Soc. Am. Bull.*, **88**, 507-530, 1977.
- Ballard, R. D., T. H. Van Andel, and R. T. Holcomb, The Galapagos Rift at 86°W, 5, Variations in volcanism, structure, and hydrothermal activity along a 30-kilometer segment of the rift valley, *J. Geophys. Res.*, **87**, 1149-1161, 1982.
- Bischoff, J. L., and F. W. Dickson, Seawater-basalt interaction at 200°C and 500 bars: Implications for origin of sea-floor heavy-metal deposits and regulation of seawater chemistry, *Earth Planet. Sci. Lett.*, **25**, 385-397, 1975.
- Cann, J. R., D. K. Winter, and R. G. Pritchard, A hydrothermal deposit from the floor of the Gulf of Aden, *Mineral. Mag.*, **41**, 193-199, 1977.
- Carnahan, B., H. A. Luther, and J. O. Wilkes, *Applied Numerical Methods*, John Wiley, New York, 604 pp., 1969.
- Cathles, L. M., An analysis of the cooling of intrusives by groundwater convection which includes boiling, *Econ. Geol.*, **72**, 804-826, 1977.
- Corliss, J. B., J. Dymond, L. I. Gordon, J. M. Edmond, R. P. Von Herzen, R. D. Ballard, K. Green, D. Williams, A. Bainsbridge, K. Crane, and T. H. Van Andel, Submarine thermal springs on the Galapagos Rift, *Science*, **203**, 1073-1083, 1979.
- Crane, K., and R. D. Ballard, The Galapagos Rift at 86°W, 4, Structure and morphology of hydrothermal fields and their relationship to the volcanic and tectonic processes of the rift valley, *J. Geophys. Res.*, **85**, 1443-1454, 1980.
- Crerar, D. A., J. Namson, M. S. Chyi, L. Williams, and M. D. Feigenson, Mangiferous cherts of the Franciscan Assemblage, I, General geology, ancient and modern analogues, and implications for hydrothermal convection at oceanic spreading centers, *Econ. Geol.*, **77**, 519-540, 1982.
- Davis, E. E., and C. R. B. Lister, Fundamentals of ridge crest topography, *Earth Planet. Sci. Lett.*, **21**, 405-413, 1974.
- Fehn, U., and L. M. Cathles, Hydrothermal convection at slow-spreading mid-ocean ridges, *Tectonophysics*, **55**, 239-260, 1979.
- Green, K. E., Geothermal processes at the Galapagos Spreading Center, Ph. D. thesis, 232 pp., Woods Hole Oceanogr. Inst., Woods Hole, Mass., 1980.
- Green, K. E., R. P. Von Herzen, and D. L. Williams, The Galapagos Spreading Center at 86°W: A detailed geothermal field study, *J. Geophys. Res.*, **86**, 979-986, 1981.
- Hartline, B. K., and C. R. B. Lister, Topographic forcing of supercritical convection in a porous medium such as the oceanic crust, *Earth Planet. Sci. Lett.*, **55**, 75-86, 1981.
- Hey, R., Tectonic evolution of the Cocos-Nazca spreading center, *Geol. Soc. Am. Bull.*, **88**, 1404-1420, 1977.
- Jenkins, W. J., J. M. Edmonds, J. B. Corliss, Excess ³He and ⁴He in Galapagos submarine hydrothermal waters, *Nature*, **272**, 156-158, 1978.
- Johnson, D. M., Fluid permeability of oceanic basalts, *Initial Rep. Deep Sea Drill. Proj.*, **51-53**, 1473-1477, 1980.
- Klitgord, K. D., and J. D. Mudie, The Galapagos Spreading Center: A near-bottom geophysical study, *Geophys. J. R. Astron. Soc.*, **38**, 563-586, 1974.
- Langseth, M. G., K. Becker, M. Hobart, and R. P. Von Herzen, Thermal regime of the oceanic crust on the flank of the Costa Rica rift (abstract), *Eos Trans. AGU*, **62**, 308, 1981.
- Lister, C. R. B., On the thermal balance of a mid-ocean ridge, *Geophys. J. R. Astron. Soc.*, **26**, 515-535, 1972.
- Lister, C. R. B., 'Active' and 'passive' hydrothermal systems in the oceanic crust. Predicted physical conditions, in *The Dynamic Environment of the Ocean Floor*, edited by K. A. Fanning and F. T. Manheim, pp. 441-470, Lexington Books, Lexington, Mass., 1981.
- Lonsdale, P., and K. D. Klitgord, Structure and tectonic history of the eastern Panama Basin, *Geol. Soc. Am. Bull.*, **89**, 981-999, 1978.
- Macdonald, K. C., K. Becker, F. N. Spiess, and R. D. Ballard, Hydrothermal heat flux of the 'Black Smoker' vents on the East Pacific Rise, *Earth Planet. Sci. Lett.*, **48**, 1-7, 1980.
- Maris, C. R. P., and M. L. Bender, Upwelling of hydrothermal solutions through ridge flank sediments shown by pore water profiles, *Science*, **216**, 623-626, 1982.
- Mottl, M. J., Metabasalts, axial hot springs, and the structure of hydrothermal systems at mid-ocean ridges, *Geol. Soc. Am. Bull.*, in press, 1982.
- Oldenburg, D. W., A physical model for the creation of the lithosphere, *Geophys. J. R. Astron. Soc.*, **43**, 425-451, 1975.
- Parsons, B., and J. G. Sclater, An analysis of the variation of ocean floor bathymetry and heat flow with age, *J. Geophys. Res.*, **82**, 803-827, 1977.
- Ribando, R. J., K. E. Torrance, and D. L. Turcotte, Numerical models for hydrothermal circulation in the oceanic crust, *J. Geophys. Res.*, **81**, 3007-3012, 1976.
- Rona, P. A., R. N. Harkison, B. G. Bassinger, R. B. Scott, and A. Nalwalk, Tectonic fabric and hydrothermal activity on the Mid-Atlantic Ridge crust (lat. 26°N), *Geol. Soc. Am. Bull.*, **87**, 661-674, 1976.
- Sayles, F. L., and W. J. Jenkins, Advection of pore fluids through sediments in the equator-

- ial East Pacific, Science, 217, 245-248, 1982.
- Seyfried, W., and J. L. Bischoff, Hydrothermal transport of heavy metals by seawater: The role of seawater/basalt ratio, Earth Planet. Sci. Lett., 34, 71-77, 1977.
- Sleep, N. H., Formation of ocean crust: Some thermal constraints, J. Geophys. Res., 80, 4037-4042, 1975.
- Sleep, N. H., and T. J. Wolery, Egress of hot water from mid-ocean ridge hydrothermal systems: Some thermal constraints, J. Geophys. Res., 83, 5913-5922, 1978.
- Williams, D. L., R. P. Von Herzen, J. G. Sclater, and R. N. Anderson, The Galapagos spreading center: Lithospheric cooling and hydrothermal circulation, Geophys. J. R. Astron. Soc., 38, 587-608, 1974.
- Williams, D. L., T. C. Lee, R. P. Von Herzen, K. E. Green, and M. A. Hobart, A geothermal study of the Mid-Atlantic Ridge near 37°N, Geol. Soc. Am. Bull., 88, 531-540, 1977.
- Williams, D. L., K. E. Green, T. H. Van Andel, R. P. Von Herzen, J. R. Dymond, and K. Crane, The hydrothermal mounds of the Galapagos Rift: Observations with DSRV Alvin and detailed heat flow studies, J. Geophys. Res., 84, 7467-7484, 1979.
- Wolery, T. J., and N. H. Sleep, Hydrothermal circulation and geochemical flux at mid-ocean ridges, J. Geol., 84, 249-275, 1976.

(Received March 8, 1982;
accepted October 15, 1982.)